Ivanova, ME.; Deibert, W.; Marcano, D.; Escolástico Rozalén, S.; Mauer, G.; Meulenberg, WA.; Bram, M.... (2019). Lanthanum tungstate membranes for H-2 extraction and CO2 utilization: Fabrication strategies based on sequential tape casting and plasma-spray physical vapor deposition. Separation and Purification Technology. 219:100-112. https://doi.org/10.1016/j.seppur.2019.03.015

Lanthanum tungstate membranes for H_2 extraction and CO_2 utilization: fabrication strategies based on sequential tape casting and plasma-spray physical vapor deposition

M.E. Ivanova[a,b]*, W. Deibert[a,b], D. Marcano[a,b], S. Escolástico[c], G. Mauer[a,b], W.A. Meulenberg[a,b,d], M. Bram[a,b], J.M. Serra[c], R. Vaßen[a], O. Guillon[a,b]

[a] *Forschungszentrum Jülich GmbH, Institute of Energy and Climate Research IEK-1: Material Synthesis and Processing, 52425-Jülich, Germany*

[b] *Jülich Aachen Research Alliance: JARA-Energy, Forschungszentrum Jülich GmbH, D-52425 Jülich, Germany*

[c] *Instituto de Tecnología Química (Universitat Politècnica de València-Consejo Superior de Investigaciones Cientifícas), Av. Los Naranjos s/n, E-46022 Valencia, Spain*

[d] *University of Twente, Faculty of Science and Technology, Inorganic Membranes, P.O. Box 217, 7500 AE Enschede, The Netherlands*

*** Corresponding Author**

Dr. Chem. Eng. Mariya E. Ivanova

Forschungszentrum Jülich GmbH

Institute of Energy and Climate Research IEK-1: Materials Synthesis and Processing

52425-Jülich, Germany

Phone: 0049-(0)-2461-615194

Fax: 0049-(0)-2461-612455

E-mail: m.ivanova@fz-juelich.de

Abstract

At the focus of energy conversion efficiency and decreasing greenhouse gas emissions from power generation and energy-intensive industries, membrane technologies for H_2 extraction and CO_2 capture/utilization become pronouncedly important. In this context, the integration of mixed protonic-electronic conducting (MPEC) ceramic membranes in H_2 extractors (as fuel) or H_2/CO_2 consumption (as raw materials for chemical production) would account for high environmental and economic impact. MPEC ceramic membranes may be therefore of interest for integrated gasification process, specifically in water gas shift reactors (T>600°C) and catalytic membrane reactors. Materials largely under focus are Lanthanum tungstates (LaWO), which exhibit appreciable protonic conductivity at intermediate temperatures, non-blocking grain boundaries, n-type electronic conductivity (under reducing atmosphere), good sinterability and stability in H_2S, CO/CO_2 and steam in comparison to zirconate-cerate solid solutions. All-ceramic ($LaWO_{mem}/LaWO_{sub}$;$LaWO_{mem}/MgO_{sub}$) and metal supported ($LaWO_{mem}/Crofer_{sub}$) asymmetric membrane assemblies were developed by means of sequential tape casting and plasma spray-physical vapor deposition (PS-PVD), respectively. The successful employment of these two complex methods for membrane manufacturing represents the core in further designing and pursuing strategies for integration of all-ceramic or ceramic-metallic assemblies in membrane modules/reactors. The present work therefore addresses fabrication aspects for achieving defect free LaWO membranes on porous ceramic and porous metallic substrates. Formation of LaWO cubic phase, gas tightness of the functional layers and stability of the structures could be achieved for all-ceramic and ceramic-metallic assemblies. This study encompasses furthermore insights on the fabrication parameters (e.g. plasma composition (for ceramic-metallic assemblies); sintering behaviour (for all-ceramic assemblies)) and understanding their correlation to reach desired material/membrane composition and functional properties.

Keywords: *Solid State Proton Conductors, Ceramic Mixed Protonic-Electronic Conductors, Lanthanum Tungstate Membranes, Metal Supported Ceramic Membranes, Crofer22APU, H_2 Separation, CO_2 Utilization, Membrane Reactors, Tape Casting, PS-PVD*

1. Introduction

The world's rapidly growing energy demand is satisfied mainly by exploiting oil, coal and natural gas as conventional sources of energy. Unfortunately, fossil fuels mining and exploitation cause environmental pollution by releasing vast amounts of CO_2, other greenhouse gases, and dust into the atmosphere. The demand for improving power generation efficiency and reducing pollutions has been attracting both scientific and industrial interest in the recent years, aiming to develop sustainable and more environmental-friendly technologies in relatively short terms. Therefore, novel and reliable concepts are required to enable their implementation in power generation and chemical production. Continuous replacement of fossils with renewable sources is ultimately envisaged as long term targeted scenario [1].

Due to the increasing importance of H_2 as a green alternative to the conventional energy sources, recognized also as "fuel of the future", which would have great social impact and economical relevance, H_2-related technologies integrated into intermediate- and high-temperature industrial processes emerge as a hot topic. On the other side, gas separation and chemical conversion by inorganic membranes for energy applications is a growing field with respect to the high efficiency of membrane-based processes [2,3]. Membrane processes can be efficiently integrated into many advanced system concepts for generation of H_2 fuel for mobile and stationary applications (steam electrolysers, WGS reactors, H_2 extractors and O_2 injection in catalytic processes), efficient and clean conversion of chemical to electrical energy (fuel cells, H_2 turbines), utilization of H_2 and CO_2 in chemistry and petro-chemistry (catalytic membrane reactors) [4-11].

H_2 permeable membranes are therefore a key element in improving the energy conversion efficiency and decreasing the greenhouse gas emissions from electricity generation, i.e. by capturing and utilizing CO_2 in chemical reactions and/or moving towards hydrogen-based systems by extracting highly pure H_2 from gas mixtures. In this context, the integration of robust and durable H_2-permeable ceramic membranes with high performance operating at elevated temperature (400-900 °C) allows achieving separation and/or chemical reaction in specific industrial processes. Such integrative membrane approach of *in situ* H_2 extraction and/or consumption in a chemical reaction would shift the thermodynamic equilibrium towards product formation, hence intensifying the process and significantly increasing per-pass product yield while reducing the efficiency losses and final product costs. In this context, scientific community faces the challenge of identifying, developing and exploring stable and well performing ceramic membrane materials for variety of chemical reactions, as well as to develop optimal reactor

designs, which could be then exploited with high conversion rates and overall process efficiency.

Specific application field sets particular requirements in terms of membrane stability. But generally membrane materials need to retain their phase and chemical composition at elevated temperatures in atmospheres possibly containing H_2, H_2O, CO, CO_2, CH_4, SO_x, H_2S, different levels of ash. Such extreme operating environments are critical for the majority of H_2 selective material classes, leading to material decomposition, membrane disintegration and performance degradation. Hydrogen permeable ceramic membranes exhibit certain advantages over different types of membranes (Fig. 1) such as robustness, high thermal and hydrothermal stability (compared to polymers, Ag-Pd, SiO_2, Carbon-SiO_2 molecular sieves for CO_2/H_2 separation), as well as better chemical stability (no H_2-induced embrittlement and sulfur poisoning particularly critical for Pd-based membranes, typically applicable up to 500 °C) [12-15]. Compared to the well-established Pd-Ag H_2-permeable metallic membranes, the material costs of ceramics are lower. In addition to material-related performance and stability characteristics, intensification of the process depends on active membrane surface, optimal gas supply to the membrane reacting side, as well as on suitable sealing technology.

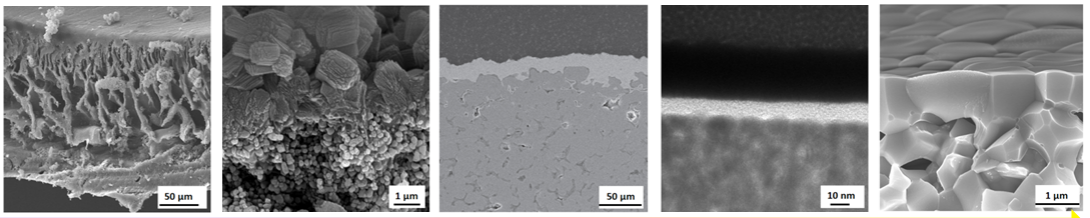

Type / Property	Dense Polymer	Microporous Ceramic	Dense Metallic	Porous Carbon	Dense Ceramic
Example material	Organic Polymers e.g. Nafion, PEEK	SiO_2, Al_2O_3, ZrO_2, TiO_2, Zeolites	Pd-alloys e.g. Pd-Au, Pd-Cu	Carbon	Proton conductors e.g. $SrCeO_3$, $BaCeO_3$
Transport Mechanism	Solution/Diffusion	Molecular sieving	Solution/Diffusion	Surface diffusion/ Molecular sieving	Solution/Diffusion
Poisoning/ Stability issues	HCl, SO_x,CO_2/swelling, densification	Stability in presence of H_2O vapour	H_2S, HCl, CO/phase transition, embrittlement	Strong vapours, organics	H_2S/stability in CO, CO_2
H_2 Selectivity	Low to moderate	Moderate	Very high	Low to moderate	Very high
H_2 Flux	Low to moderate	High	High	Moderate	Moderate

Figure 1. Comparison of different membrane types for H_2 separation

The present work presents recent insights on fabrication and characterization of Lanthanum tungstate (LaWO) membranes by two parallel technologies: sequential tape casting and plasma spray-physical vapor deposition (PS-PVD). These two fabrication strategies allow for different

concepts of membrane integration in membrane extractors and reactors leading to all-ceramic or ceramic-metallic assemblies, respectively.

The candidate membrane material LaWO exhibits appreciable mixed protonic-*n*-type electronic conductivity under reducing atmospheres at intermediate to high temperatures [16], non-blocking grain boundaries, good sintering ability and stability in H_2S, CO/CO_2 and steam [17-19]. Cubic phase formation and gas tightness of the LaWO functional layers was a subject of intensive investigation within the present work, which encompasses furthermore insights on the fabrication parameters (e.g. plasma composition (for ceramic-metallic assemblies), sintering behaviour (for all-ceramic assemblies)) and understanding their interplay to reach desired material/membrane functional properties.

Asymmetric membrane systems were developed as *i)* full ceramic assemblies consisting of $LaWO_{mem}$ on $LaWO_{sub}$ and $LaWO_{mem}$ on MgO_{sub}, and as *ii)* ceramic membranes supported on porous metal structures ($LaWO_{mem}$ on $Crofer_{sub}$). Single LaWO phase membranes with high gas tightness could be finally achieved on both porous ceramic and porous metallic substrates. Despite the high complexness of the PS-PVD processing compared to the tape casting, this approach leads to important benefits in terms of membrane sealing and joining to reactor metal frames and circumvents the limitation of high sintering temperatures required in all-ceramic processing.

Theoretical Background

1.1. Mixed protonic-electronic conductors

Solid state oxide ceramics are complex systems in terms of their structure and chemical composition, which determine the nature of the charge carriers contributing to their electrical properties. On the other hand, their interaction with the environment aiming for establishing of equilibrium controls to a large extent the formation of charged species.

Like that, protons are incorporated into the crystal lattice due to the hydration of the material according to Eq. 1 in Kröger-Vink notation:

$$H_2O_{(g)} + v_O^{\bullet\bullet} + O_O^X \rightarrow 2OH_O^{\bullet} \qquad \text{(Eq. 1)}$$

Protons are mobile and by means of lattice diffusion give rise to certain levels of protonic conduction in the solid oxide ceramics.

Furthermore, electronic conduction may be boosted by the substitution with metallic cations with variable valence [20-22].

Finally, due to the fact that ceramics of interest as H_2 separation membranes are oxide based systems, oxygen ions contribute to the overall conduction by means of lattice diffusion under elevated temperatures.

Transport of species across the membrane depends on the environmental conditions (hydration degree, temperature, atmosphere composition), therefore particularly influenced by partial pressures of gases at the two sides of the membrane. In fact, oxygen ions can be transported from the sweep side (p_{H2} lower than in the feed side but p_{O2} higher than the p_{O2} in the feed stream) to the feed side (H_2-containing mixture with high p_{H2} but low p_{O2}), as depicted in the Fig. 2. Usually, humidity is required on both sides of the membrane to boost the overall performance.

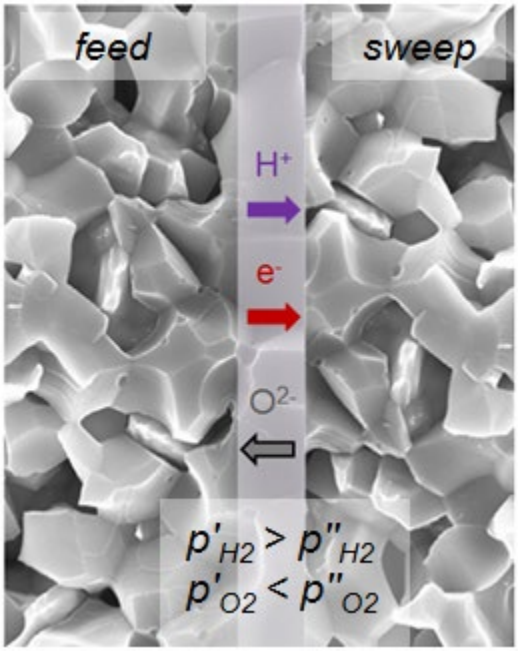

Figure 2. Schematic of a gas-tight ceramic membrane between two porous layers. The transport direction for the predominant charge species across the membrane is depicted. Left-hand side is considered as H_2-containing mixture feed side (high p_{H2} side), while the right-hand side represents the sweep side (low p_{H2} side).

According to the description above, due to the gas partial pressure, net flux of H_2 will result out of the mixed protonic-electronic conducting membrane, according to the Wagner theory (Eq. 2), which takes more complex form in the case of mixed protonic-oxygen ionic-electronic conducting membrane (Eq. 3).

$$j_{H_2} = \frac{-RT}{2F^2 L} \int_I^{II} \sigma_{H^+} t_{e^-} d \ln p_{H_2} \qquad \text{(Eq. 2)}$$

$$j_{H_2} = \frac{-RT}{2F^2 L} \int_{I}^{II} \sigma_{H^+} \left[t_{e^-} d \ln p_{H_2} + t_{O^{2-}} d \ln p_{H_2O} \right] \qquad \text{(Eq. 3)}$$

As seen from the two equations above, aiming for higher protonic and electronic (ambipolar) conduction levels, major strategies for tailoring material functional properties intensively considered in membrane development are *i)* substitution of lattice constituents and *ii)* combining two phases with good compatibility and complementary properties. Apart from the material-related properties, process parameters (gas pressures, temperature) and decreasing membrane thickness (L) have importance in achieving better overall performance of the H_2 permeable dense ceramic membrane. Therefore exploring the suitability, efficiency and reproducibility of fabrication approach has significant importance too, along with the scale-up to industrially relevant sizes.

1.2. Lanthanum Tungstate LaWO ($La_{28-x}W_{4+x}O_{54+\delta}$)

Lanthanum tungstate with general formula $La_{6-x}WO_{12-\delta}$ ($0.3<x<0.7$) belongs to the defective-fluorite structural type. This material provides the highest protonic conductivity amongst the number of reported rare earth tungstates [23,24]. In addition, due to its electronic properties and high thermo-chemical stability at elevated temperatures it has the potential to meet the challenges of a real membrane application.

Despite several attempts to solve accurately the crystal structure [25,26], this family of materials exhibits polymorphism and extremely subtle distortions. Therefore, the high level of structural complexity with lacking clarity over the last decade leading to significant deficiency in understanding on how structure influences functional properties. Finally, realistic models of the average and local structures have been developed disclosing the particular lattice symmetry, degree of cation ordering and location of oxygen vacancies [27,28]. Furthermore, crystal structure and hydration properties of Re and Mo (up to 20 mol.%) substituted LaWO were thoroughly investigated [29,30], due to the large potential of LaWO after substitution with cations of mixed valence (increased electronic conduction). As reported previously, La site substitution for a number of elements has less impact on achieving improved H_2 flux performance [22,31,32]. However, after partial substitution on W site, specifically with Mo and Re, higher levels of ambipolar conduction (electronic term increased) could be achieved and substantially higher H_2 fluxes were reported (7- to 10-fold increase for Mo and Re-substituted LaWO at an intermediate temperature of 700°C) [20]. For comparison, similar values of H_2 flux can be achieved by the non-substituted LaWO material but only at working temperature of 950 °C. Theoretical estimation of the performance shows that a value of 1 ml/min·cm^2 at 700 °C could

be achieved with a Re substituted LaWO membrane of 70 μm thickness and a Mo substituted LaWO membrane of 30 μm thickness (under the assumption that there is no gas transport limitations across the porous substrate). For achieving such thicknesses, functional membrane layer needs to be supported onto chemically and thermally compatible porous substrate with porosity above 30% so that the gas flow to and out of the membrane is not impeded by insufficiency of gas access and driving force.

1.3. Fabrication Methods

Most of the fabrication efforts have been focused on developing LaWO membranes (both non-substituted material, as well as Re and Mo substituted LaWO) by tape casting [33,34]. This method allows for fabrication of scalable asymmetric membrane structures with high geometrical (planar) flexibility, reproducibility and process efficiency. It enables furthermore the combination of different materials in green state, either all-ceramic or ceramic-metallic, however displaying limitation specifically for ceramic-metallic assemblies due to the required further high temperature processing (sintering) under oxidizing conditions. Therefore, aiming to achieve ceramic-metallic assemblies for further conventional integration in membrane reactors, PS-PVD was considered a very suitable technique since no high temperature co-firing is required, only annealing step at 900-1000 °C [35,36]. Processing of ceramic-metallic assemblies by means of PS-PVD enables conventional integration (welding) of such components in metal constructions [37]. Major practical difficulties of the method are the precise control over complex process parameters to achieve desired stoichiometry along with the high investment costs to acquire the respective equipment.

2. Experimental part

2.1. Membrane fabrication by tape casting

2.1.1. Starting powders

LaWO powder synthesized via the solid state reaction (SSR)

The powder used for membrane preparation was synthesised via the solid state reaction (SSR). For this purpose, stoichiometric amounts of La_2O_3 (99.999%, Sigma Aldrich) and WO_3 (99.995%, Sigma Aldrich) were milled in ethanol. After drying, the powder mixture was heated at 1500 °C for 12h to accomplish the solid state reaction. The resulting powder was additionally milled in a planetary ball mill and sieved (32 μm mesh size). The mean particle size d_{50} of 0.8 μm and the specific surface area of 1.9 m^2/g were estimated by means of laser diffraction and BET analysis.

LaWO powder synthesized via the modified Pechini method

Due to its higher stoichiometric precision Pechini method was used to synthesize 20 mol.% Re and 20 mol.% Mo substituted LaWO. As precursors, $LaN_3O_9 \cdot 6H_2O$ (lanthanum nitrate, Merck), $H_{42}N_{10}O_{42}W_{12} \cdot H_2O$ (ammonium tungstate, Sigma Aldrich), $HReO_4$ (Re acid, Alfa Aesar), $H_{24}Mo_7N_6O_{24}$ (ammonium molybdate, Sigma Aldrich) were used in addition to $C_6H_8O_7 \cdot H_2O$ (citric acid, Merck) and $C_2H_6O_2$ (ethylenglycol, Merck). Synthesis procedure is described elsewhere [31,38]. For complete removal of organics a heat treatment at 900 ºC was carried out. To adapt powder properties to the tape casting process, additional pre-calcination and milling steps were carried out.

LaWO powder (commercial)

As starting powder for substrate preparation was used a commercially available LaWO with a La/W ratio of 5.4 (CerPoTech, Norway) produced by spray pyrolysis and calcined at 600 °C [39]. In order to adjust the specific surface area (initially 7 m²/g) and the respective sintering activity of the commercial powder, additional thermal treatment and milling step were necessary.

MgO powder (commercial)

MgO powder (Sigma Aldrich) with d_{50}=7.7 µm and specific surface area of 66 m²/g was used to shape porous substrates as alternative to LaWO. As in the case of LaWO commercial powder, powder properties were tailored first by annealing and milling before using in the tape casting process.

2.1.2. Cer-cer assemblies by tape casting

Sequential tape casting was performed on a micro-tape casting bench KAROcast300-7 by KMS Automation GmbH Germany. More details on the slurry preparation can be found elsewhere [34,40]. Before the slurries were used in the tape-casting experiments, they were homogenised and de-aired by applying a vacuum within the mixing device. Supports were cast using solvent-based slurry with 10 wt.% rice starch (particle size 2-8 µm) as pore former. Blade gap of 1mm resulted in substrate thickness of ca. 400µm in the final sintered state (1500 °C, 3h), while gap of 100 µm resulted in 30 µm thick membrane layer.

The sequential tape casting in brief consists of casting first the membrane layer onto the PET foil (thickness 100 µm, Karo Electronics Vertriebs GmbH, Germany), which moves with controlled speed into the vented chamber. After the complete drying of the membrane layer, the substrate layer is cast on top so that in most of the cases defect-free functional membrane layers can be produced.

2.2. Membrane fabrication by PS-PVD

2.2.1. LaWO powder feedstock

The feedstock material $La_{6-x}WO_{12-\delta}$ was provided by Oerlikon Metco, Wohlen, Switzerland. Particle size distribution was estimated by laser diffraction with d_{10}=7 µm, d_{50}=11 µm, and d_{90}=17 µm. Single phase cubic LaWO was ascertained by Rietveld refinement of X-ray diffraction (XRD) patterns. Prior to spraying the as-delivered powder with spherical morphology a drying step was conducted at 80 °C for 24 h in air to avoid agglomeration and to favor the flowability of the powder.

2.2.2. Manufacturing of porous metallic supports

Crofer22APU stainless steel was selected as support material for the LaWO functional membrane layers due to their well matching coefficients of thermal expansion: $CTE_{Crofer22APU}$ of $12.3 \cdot 10^{-6}$ K^{-1} and CTE_{LaWO} of $11\text{-}12 \cdot 10^{-6}$ K^{-1}. No intermediate layers were applied. Substrates were manufactured by means of the tape casting on casting bank FGA500-SAMA, Germany. As starting powder, gas atomized ferritic steel Crofer22APU powder by H.C. Starck, Germany (powder fraction with a median of d_{50}=13.3 µm) was used. An alcohol-based slurry with solid load of 88 wt.% was produced, using ethanol as solvent and a combination of binder (Mowital, Kuraray, Japan) and plasticizing agents. Slurry viscosity was 20 ± 2 Pa·s at shear rate of 1.8 s^{-1}. Green tape thickness after drying was in the range of 1150-1200 µm and samples with dimensions 70x70mm^2 were cut out of this tape. Thermal treatment included three steps: de-binding at 600 °C for 30 min, pre-sintering at 900 °C in Ar and final sintering at 1100 °C for 2 h in Ar. The final thickness of the sintered samples was estimated to be 0.87-1.03 mm with an average porosity of ca. 30% (based on SEM image analysis). To shape round samples, laser cutting was applied to a final diameter of 15 mm.

2.2.3. Cer-met assemblies by PS-PVD

The coating was deposited by means of the Multicoat PS-PVD system (Oerlikon Metco, Wohlen, Switzerland) with an O3CP torch. A current of 2000A resulting in a torch input power of 90 kW at a chamber pressure of 250 Pa (2.5 mbar) were used. The plasma spray parameters intended to obtain gas tight ceramic membranes were adjusted accordingly to our previous work [41-43]. In brief, plasma consists of Ar and He fed with two different ratios Ar:He=100:30 slpm and 110:20 slpm (slpm: standard liters per minute). In some cases extra amounts of oxygen were supplied to the chamber to account for oxygen stoichiometry. Two spray distances of 900 and 1000 mm and coating times of 3 min were chosen resulting in layers with thickness of 40 to 60 µm. It should be mentioned here, that for the manufacturing of dense coatings the deposition of fast and perfectly molten splats instead of gas phase deposition is used. A sample holder with a metallic mask was used, so that samples were kept in position without being constrained

during heating and cooling. At the same time, the heat flow from the samples was ensured. After spraying, the samples were annealed at 900 °C for 3h in Ar and air.

3. Characterization techniques

3.1. Physical properties of the powders

The particle size distribution (PSD) and specific surface area (BET) [44] of the starting powders to prepare asymmetric structures were carefully monitored and controlled respectively with Horiba LA-950 V2 by Retsch Technology and area-meter from Ströhlein with N_2 as measurement gas.

3.2. Chemical and phase composition

The chemical composition of the membranes was determined using Inductively Coupled Plasma-Optical Emission Spectrometry (ICP-OES). Also, the content of oxygen was measured and the stoichiometry was calculated. The error in this measurement was ± 3%.

X-ray diffraction (XRD, D4 Endeavor - Bruker AXS with Cu-Kα radiation) was performed to determine the phases present in the LWO coating in “as-sprayed” and in “as-annealed” in Ar or Air state. The TOPAS V 4.2 software was used for Rietveld analysis. This was performed by varying the sample displacement, the lattice parameter, profile shape parameters and the overall isotropic thermal parameter. Phase identification was carried out with ICDD PDF2-Database (Release 2004), ICSD Database (Release 2017) and X’Pert Highscore Plus (by PANalytical). The reference patterns correspond to the cards ICSD 252211 ($La_{6.75}W_{1.25}O_{13.5}$), PDF No. 01-074-2430 ($La_2O_3$) and ICSD 247427 ($La_6W_2O_{15}$) for phase identification. These references were then used as a starting model for the Rietveld analysis.

3.3. Thermal properties

The sintering behaviour of tape cast LaWO layers was studied with a TOMMIplus optical dilatometer by Fraunhofer ISC, Würzburg, Germany. The sample with known dimensions was positioned on the sample holder within the instrument chamber, where it was gradually heated (heating ramps of 1–5 °C/min up to 1500 °C, dwell time 3h). Images of the sample silhouette were periodically recorded (every 60s) with a charge-coupled device (CCD) camera during heat treatment. To achieve high contrast, a monochromatic light source was mounted opposite to the camera. Software TOMMI online (Fraunhofer ISC, Würzburg, Germany) was used to analyse the corresponding shrinkage of the samples.

3.4. Microstructure and topography

To investigate the microstructure of tape-cast samples, scanning electron microscopy (SEM) was performed by means of Phenom electron microscope manufactured by FEI with a back-

scattered electron detector and acceleration voltage of 5 kV, as well as Zeiss Ultra 55 electron microscope with an acceleration voltage of 15 kV and a back-scattered detector. Porosity, layer thicknesses, and pore size of the samples in cross sections were quantified with AnalySIS pro software (Olympus Soft Imaging Solutions GmbH).

The shape and topography of the samples were monitored by means of a CT350 T device from Cyber Technologies using a confocal white light sensor. The *z*-resolution of the sensor was 0.1 µm and the spot size was 12 µm.

3.5. Helium (He) gas-tightness and H_2 permeation

He leakage tests were performed on sintered asymmetric membranes by means of a Pfeiffer leakage test setup. For this purpose, the samples (measured area of 1cm²) were contacted to a rubber sealing, first on the membrane side, afterwards on the substrate side, and a pressure difference of 1000 hPa was applied. The permeation was detected by a mass spectrometer in $hPa \cdot dm^3 \cdot cm^{-2} \cdot s^{-1}$. A maximal value of $1 \cdot 10^{-3}$ $mbar \cdot l \cdot cm^{-2} \cdot s^{-1}$ ($hPa \cdot dm^3 \cdot cm^{-2} \cdot s^{-1}$) was set as He leakage threshold, samples displaying values higher than that were not considered as gas-tight.

H_2 permeation tests were carried out in a double chamber quartz reactor. All the membranes were catalytically activated. Pt catalytic layer was screen-printed on both sides of the LWO bulk membrane. $LWO_{mem}/Crofer_{sub}$ and LWO_{mem}/LWO_{sub} membranes were also catalytically activated with Pt, in both, dense membrane layer (screen-printed Pt layer) and porous substrate (infiltrated Pt).H_2 was separated from a mixture of $50mL \cdot min^{-1}$ $H_2$and $50mL \cdot min^{-1}$ He by using Ar as sweep gas (flow rate of 150 ml/min). The H_2 content in the permeate side was analysed using a micro-GC Varian CP-4900 equipped with Molsieve5A and PoraPlot-Q glass capillary modules.

For the asymmetric membranes, measurements were performed with the membrane layer and the support on the feed and the sweep side, respectively.

4. Results and discussion

After optimization of process parameters, asymmetric membrane samples consisting of $LaWO_{mem}/LaWO_{sub}$; Mo-$LaWO_{mem}/LaWO_{sub}$; Re-$LaWO_{mem}/LaWO_{sub}$; $LaWO_{mem}/MgO_{sub}$; Mo-$LaWO_{mem}/MgO_{sub}$ and Re-$LaWO_{mem}/MgO_{sub}$ were fabricated by tape casting. Multilayered tapes in dry state before sintering are depicted in Fig. 3, while selected tape cast samples in sintered state and PS-PVD sprayed sample ($LaWO_{mem}/Crofer_{sub}$) are shown in Fig. 4.

Due to the different shrinkage rates of membrane and substrate tape cast layers during sintering which was thoroughly discussed elsewhere [34] fabrication of flat asymmetric membranes represents a major challenge, especially when up-scaling is considered, therefore detailed knowledge about the sintering behavior of different layers and their careful matching is required.

To ascertain the flat geometry with minimal deformations, white light topography is a main helping tool. Fig. 4d below depicts an exemplary image of a flat round shape $LaWO_{mem}/LaWO_{sub}$ after sintering.

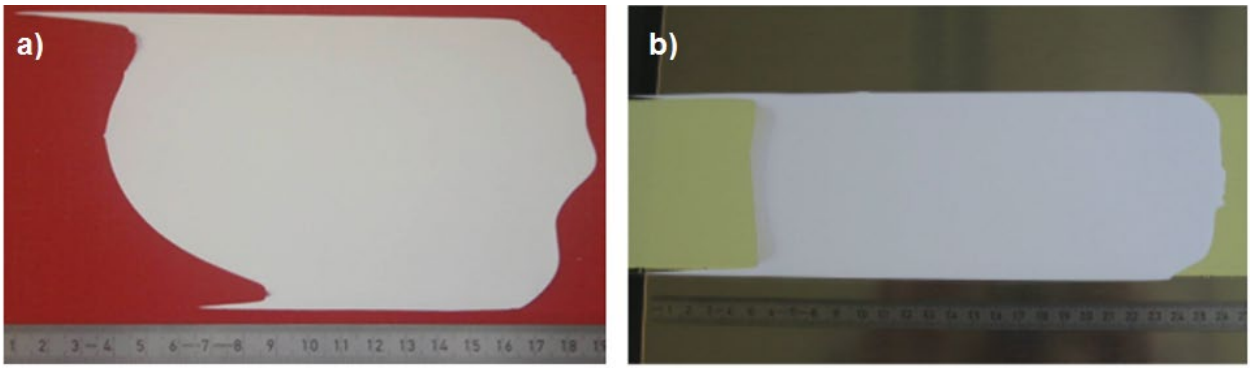

Figure 3. Images of tapes in dry state, a) LWO_{mem}/LWO_{sub} (two tapes have white colour) and b) Re-$LaWO_{mem}$ (here seen as the yellowish-greenish coloured tape)/LWO_{sub} (white tape on top)

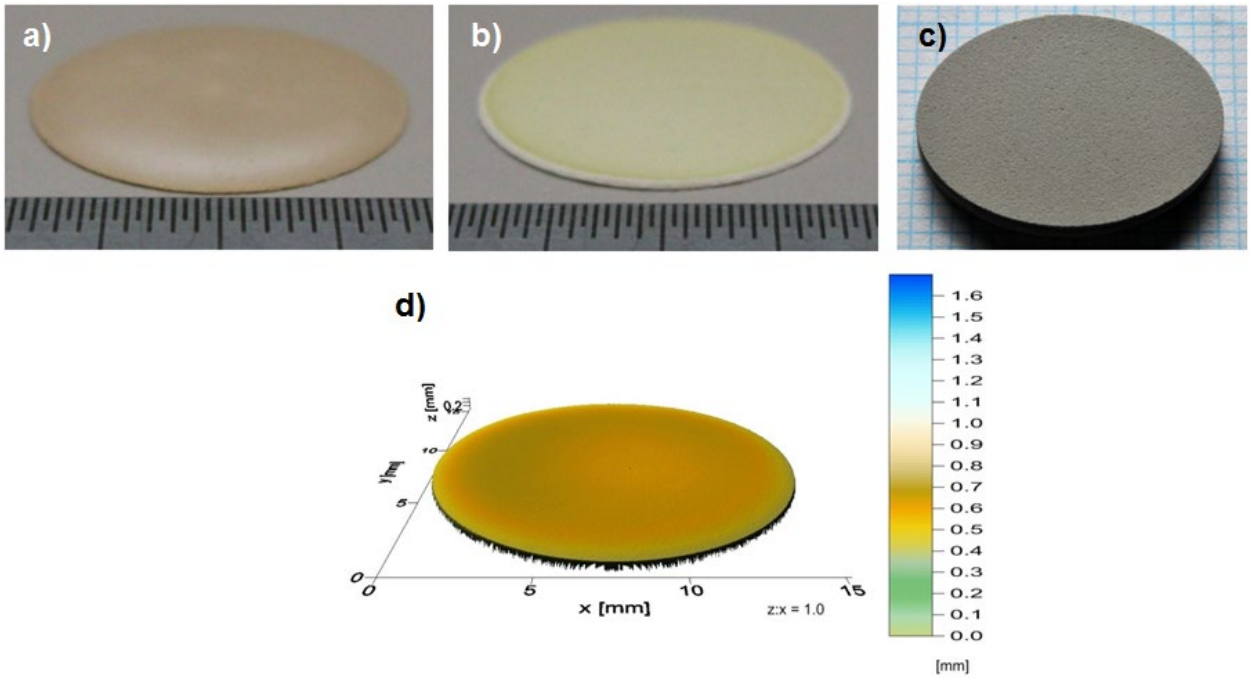

Figure 4. Images of asymmetric membranes: a) LWO_{mem}/LWO_{sub} assembly by tape casting (sintering at 1450 °C, 6h, sample not completely flat); b) LWO_{mem}/MgO_{sub} assembly by tape casting (sintering at 1450 °C, 6h); c) $LWO_{mem}/Crofer_{sub}$ by PS-PVD (annealing at 900 °C, 3h); d)

white light topographic image of LWO_{mem}/LWO_{sub} (sintering at 1450 °C, 6h, with optimized slurry recipe, flat sample was obtained)

4.1. Structural and microstructural characteristics of all ceramic assemblies

The formation of single cubic phase depends on the La/W ratio affected by the effective levels of substitution as well as on thermal processing conditions. As already demonstrated in earlier works, La/W shifted from the optimal range of 5.3-5.7, leads to formation of undesired secondary phases [25,31], especially in substituted compounds (Fig. 5) and membranes (Fig. 6). Due to the multiphase nature of the Mo-LaWO and Re-LaWO membranes obtained by tape casting, further optimization will be required before estimating the performance properties. Secondary phases in the membranes and element diffusion pathways can be clearly observed from the SEM images in Fig. 7, last schematically represented in Fig. 8.

Due to the enlarged crystal cell parameter caused by Mo substitution [45], a shift towards smaller diffraction angle can be observed, along with secondary phase formation (peak splitting in Fig. 6 a) and b)). While the starting Mo-LaWO powders contain small amounts of La_2O_3, (Fig. 5 a), b)), such segregations were not detected in the XRD pattern of the membrane. In the case of Re substitution, the XRD pattern of the membrane compared to that of the powder shows higher inhomogeneity and higher presence of secondary phases. Furthermore, the SEM analysis of the asymmetric Mo-LaWO and Re-LaWO membranes (Fig. 7b), c)), discloses small dark areas, mostly composed of the $La_6W_2O_{15}$.

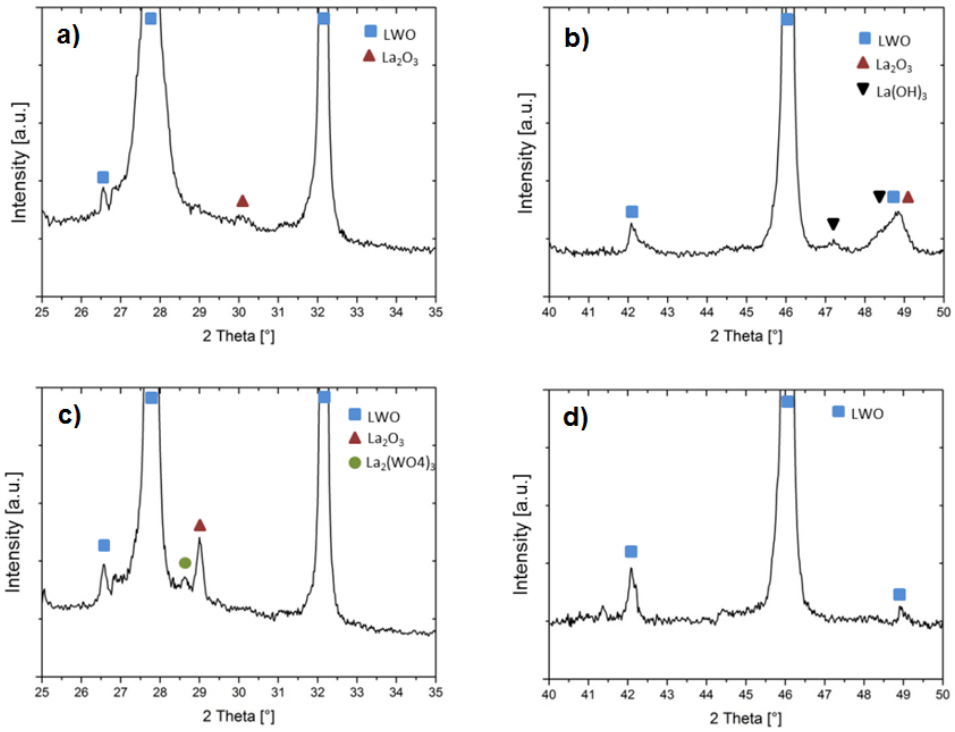

Figure 5. Excerpts of the XRD patterns of Pechini synthesized powders: a) and b) Mo-LaWO; c) and d) Re-LaWO.

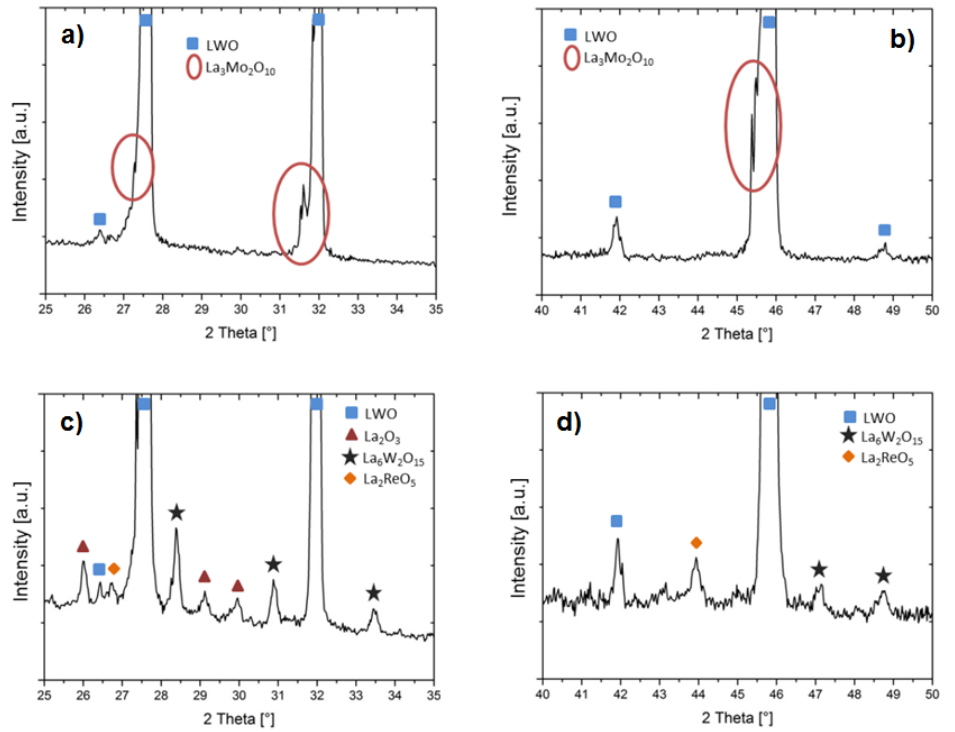

Figure 6. Excerpts of the XRD patterns of assemblies: a) and b) Mo-$LaWO_{mem}/LaWO_{sub}$; c) and d) Re-$LaWO_{mem}/LaWO_{sub}$. Sintering was carried out at 1450 °C for 6h for all samples.

In the case of MgO supported structures, diffusion of Mg towards the LaWO membrane layer was observed, as well as of La and W towards the substrate, reaching a depth of about 60 µm (Fig. 7 d), e) and Fig. 8 a), c)). For Mo-$LaWO_{mem}/LaWO_{sub}$ and Re-$LaWO_{mem}/MgO_{sub}$ assemblies diffusion depth of ca.15 µm and 20 µm for Mo and Re versus the substrate, respectively, was reached (Fig. 8 b and d)). Due to the fact that Mo and Re diffuse towards the substrate, the required La/W+Mo and La/W+Re ratios were affected leading to segregations of secondary phases, as discussed previously. In some cases (Re-$LaWO_{mem}/MgO_{sub}$, Fig. 7 f)), the membrane showed significantly decreased integrity due to impurities.

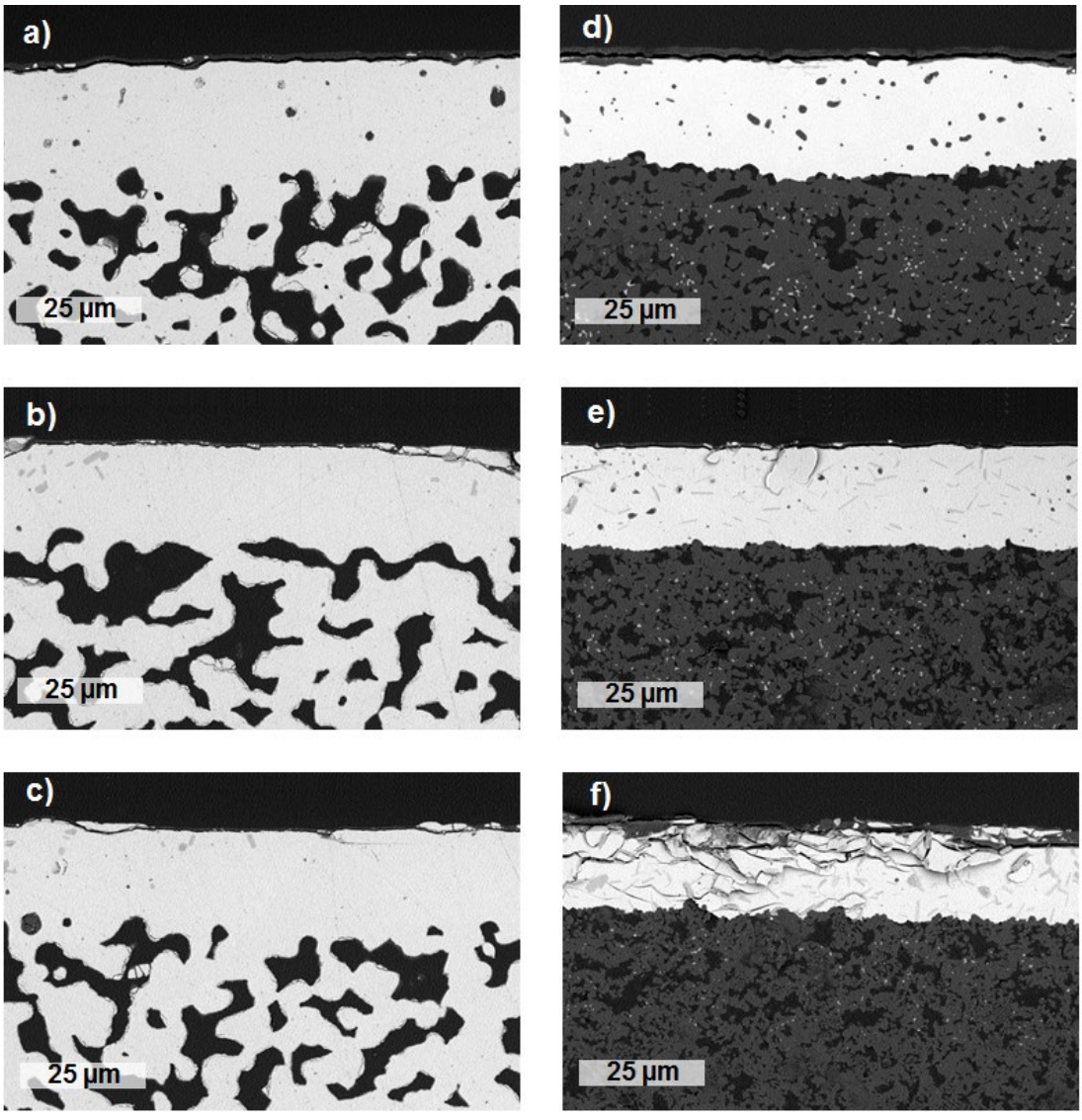

Figure 7. SEM images, polished cross-sections of assemblies manufactured via tape casting: a) $LaWO_{mem}/LaWO_{sub}$; b) Mo-$LaWO_{mem}/LaWO_{sub}$ c) Re-$LaWO_{mem}/LaWO_{sub}$; d) $LaWO_{mem}/MgO_{sub}$; e) Mo-$LaWO_{mem}/MgO_{sub}$; f) Re-$LaWO_{mem}/MgO_{sub}$. Sintering was carried out at 1450 °C for 6h for all samples. Final substrate porosity of ca. 30% and membrane He leakage of 10^{-4} to 10^{-5} mbar·l·cm^{-2}·s^{-1} were achieved. Membrane thicknesses are in the range 20-30 µm.

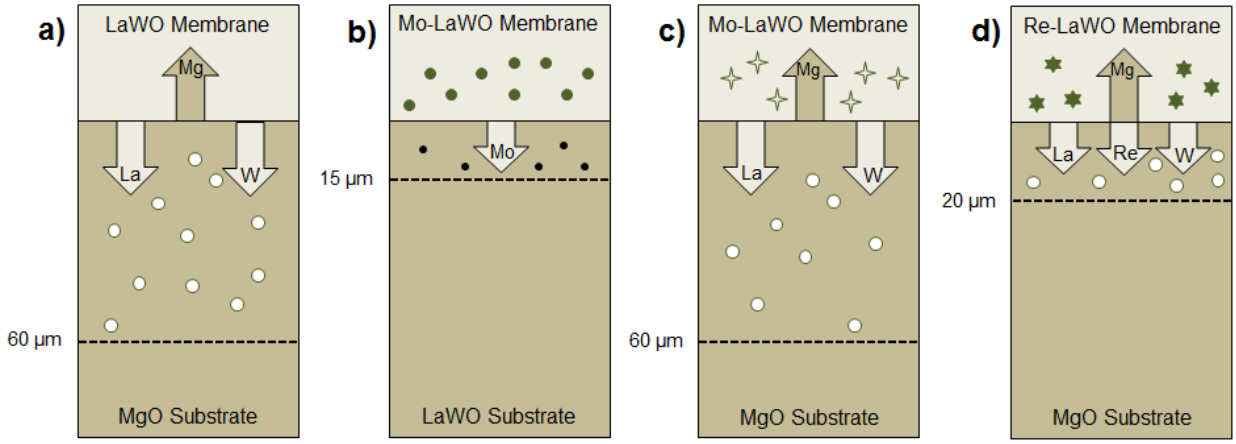

Figure 8. Schematics of cation diffusion pathways in asymmetric assemblies as secondary phase formation driving force: a) $LaWO_{mem}/MgO_{sub}$ [40]; b) Mo-$LaWO_{mem}/LaWO_{sub}$; c) Mo-$LaWO_{mem}/MgO_{sub}$; d) Re-$LaWO_{mem}/MgO_{sub}$; Different secondary phases are marked with symbols (○ La, W segregations; • $La_3Mo_2O_{10}$; ● $La_6W_2O_{15}$; ✧ and ✸ are multiple secondary phases, including La_2O_3, La_2ReO_5, $La_6W_2O_{15}$)

To summarize on microstructure, apart from the tendency to form secondary phases due to the complex compositions and sensitive La/W ratios, membranes with thickness of 25-30 µm were formed, while substrate thicknesses was about 300-400 µm after sintering (1450 °C for 6h). Final substrate porosity of ca. 30% and membrane He leakage of 10^{-4} to 10^{-5} mbar·l·cm^{-2}·s^{-1} (for defect free membranes) were achieved.

4.2. Structural and microstructural characteristics of ceramic-metallic assemblies

LaWO dense membranes sprayed on Crofer porous substrate revealed less than 5% porosity and tolerable amount of secondary phases (~2%). By that, lower temperatures (900-1000 °C) than conventionally required for sintering of LaWO (1450-1500 °C) were applied and the single cubic phase could be obtained. As the PS-PVD membrane fabrication depends on a number of process parameters, a systematic study on the effect of processing on membrane

characteristics was recently carried out and will be published soon, offering much deeper insights and analysis in this regard [46].

The cross-section of a $LaWO_{mem}/Crofer_{sub}$ assembly can be seen from the SEM micrograph in Fig. 9, which reveals homogeneous and well adhering LaWO membrane layer with thickness of about 60 µm formed onto Crofer rough surface.

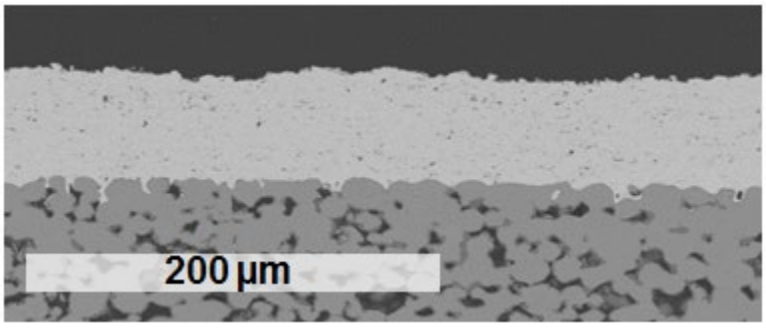

Figure 9. SEM image of $LaWO_{mem}/Crofer_{sub}$ assembly: cross section. Membrane thickness of around 60 µm

Since the LaWO pure phase formation is very sensitive on the exact La/W stoichiometry, process parameters can be used as control valves until adjusting the desired membrane quality. Fig. 10 depicts as an example two cases demonstrating the effect of annealing in Ar or air at 900 °C on the phase composition of LaWO membrane.

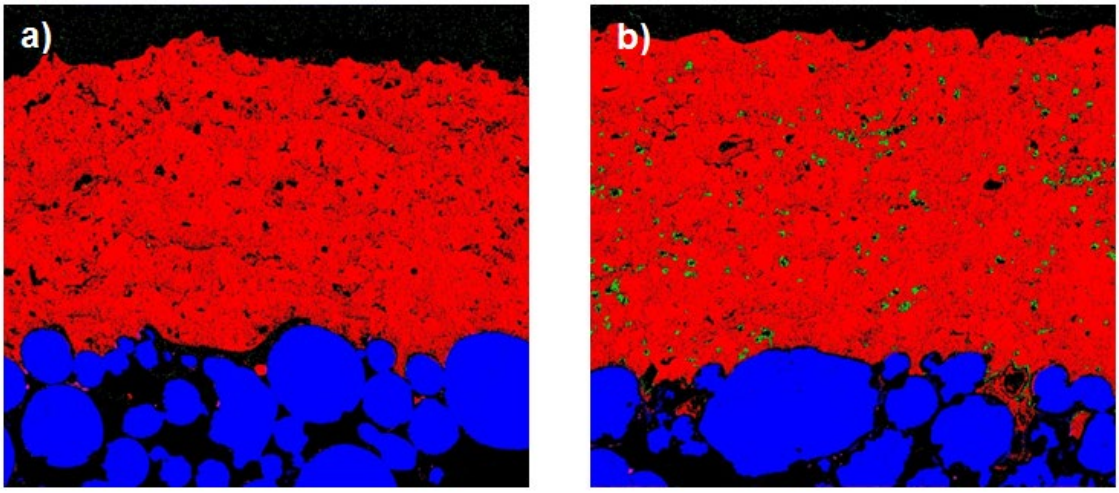

Figure 10. EBSD-image of cross sections of $LaWO_{mem}/Crofer_{sub}$ assembly: a) after annealing in Ar at 900 °C for 3h and b) after annealing in air at 900 °C for 3h for a sample prepared under addition of O_2 in the plasma chamber. LaWO phase in red, Crofer substrate in blue, secondary

phase La_2O_3 in yellow is negligible in two samples, while the segregations of $La_6W_2O_{15}$ in green are preferably formed in b).

After annealing in Ar the main cubic phase is homogeneously distributed throughout the sample and the secondary phase La_2O_3 is negligible (Fig. 10 a)). Adding O_2 during spraying affects the stability of the desired LaWO cubic phase due to interaction with oxygen vacancies, as confirmed by decrease in lattice parameter from 11.247(1) Å (for sample sprayed without additional O_2) to 11.229(1) Å. However, further annealing in air leads to formation of La_2O_3 and $La_6W_2O_{15}$ segregations (Fig. 10 b)).

4.3. Performance data

H_2 permeation under elevated temperatures was tested for LWO_{mem}/LWO_{sub} (sintered at 1450 °C for 6h in air and catalytically activated with Pt) and $LWO_{mem}/Crofer_{sub}$ (annealed in Ar). These two types of samples were selected due to their single phase composition of the membrane layer and the flat geometry enabling sealing in the test rig. We would like to mention here, that during sealing of samples, several tape cast samples broke due to the thin planar geometry (total sample thickness less than a half of mm), while some of the PS-PVD samples delaminated (membrane detached from the substrate). Regarding to the substrate porosity, the value of 30% might be not satisfactory for the optimal gas flow to and out of the tape cast membrane, however first tests of membrane performance could be carried out. As the application relevant conditions require temperature between 600-800 °C and presence of water, measurements were done in that temperature window under supply of humidity at the feed side, at the feed and sweep side or only at the sweep side. In order to promote the surface reactions, a Pt catalytic layer was screen-printed on both sides of the LWO bulk membrane. $LWO_{mem}/Crofer_{sub}$ and LWO_{mem}/LWO_{sub} membranes were also catalytically activated with Pt, in both, dense membrane layer (screen-printed Pt layer) and porous substrate (infiltrated Pt). Experimental data for bulk LaWO sample [19] under same measuring conditions show one order of magnitude lower performance. Data from these first measurements are summarized in Table 1 and need to be reproduced.

Table 1. H_2 performance under humid conditions in the sweep: summary of first data collected on LaWO bulk membrane and asymmetric membranes with different thicknesses (L_{mem}) fabricated by tape casting (LWO_{mem}/LWO_{sub}) and PS-PVD ($LWO_{mem}/Crofer_{sub}$).

	H_2 permeation ($mL \cdot min^{-1} \cdot cm^{-2}$)

Membrane	L_{mem} (µm)	650°C	700°C	750°C	800°C
LaWO bulk	900	-	-	0.02	0.03
LWO_{mem}/LWO_{sub}	25	0.007	0.025	0.065	0.107
$LWO_{mem}/Crofer_{sub}$	60	-	0.133	0.193	0.292

The first measured values summarized in the table show that decreased membrane thickness (bulk versus thin layer configuration) improves the performance as the theory predicts. Detected H_2 permeation values shown in the table are very good compared to other literature data, summary of thickness-normalized H_2 flux data is published in [47]. Bulk Y and Mn co-substituted $BaZrO_3$ at 1000 °C [48] reveals the same value as the LaWO bulk membrane at 800 °C. At 750 °C-800 °C performance significantly approaches the values measured on bulk dual phase cerate-ceria based membrane at 700 °C [47,49]. However, they are lower than the reported for an asymmetric membrane composed of a 20 µm $BaCe_{0.65}Zr_{0.20}Y_{0.15}O_{3-\delta}$–$Gd_{0.2}Ce_{0.8}O_{2-\delta}$ (BCZY–GDC) layer supported on a 600 µm porous substrate with the same composition [50]. It is worth mentioning, that this dual phase membrane consists of protonic- and electronic-conducting intercrossing phases and its performance is usually far beyond that of a single phase compound, therefore here a dual phase membrane reveals higher performance at lower temperature and much larger thickness. There is however not much available performance data on asymmetric membranes developed with the same methodology, and characterized with similar equipment and conditions, so that a reliable comparison is difficult. Furthermore, the reproducibility of the collected data on asymmetric LWO_{mem}/LWO_{sub} and $LWO_{mem}/Crofer_{sub}$ membranes needs to be ascertained. As next step, improving the performance furthermore is aimed by microstructural optimization (including substrate porosity, membrane thickness, surface activation). By doing this the potential of using single phase LaWO for H_2-separation from CO_2 and CO containing gas mixtures will be completely revealed. Finally, due to the number of advantages offered by the tape casting and PS-PVD, large scale membrane development is envisaged for subsequent integration in membrane modules and catalytic membrane reactors, so that for industrially interesting chemical processes proof of different concepts using proton conductors can be ensured.

Conclusions

The present work demonstrates the successful fabrication of gas-tight asymmetric membranes mostly consisting of LaWO cubic phase (besides the substituted LaWO compositions) formed on porous ceramic and metallic substrates. The employed fabrication methods- the tape casting

and the PS-PVD, lead to the formation of defect free functional layers only after careful adjustment of the complex fabrication parameters. First performance data collected on ceramic and metallic supported asymmetric structures revealed the high potential of LaWO membranes for H_2 separation from aggressive gas mixtures. As next steps, reproducing the performance is envisaged, as well as microstructure designing to boost the performance. Finally, scaling up of proton conducting membrane components to industrially relevant sizes will be aimed for different applications.

Acknowledgements

ProtOMem Project under the BMBF grant 03SF0537 is gratefully acknowledged. Furthermore, the authors thank Ralf Laufs for his assistance in operating the PS-PVD facility. Dr. A. Schwedt from the Central Facility for Electron Microscopy (Gemeinschaftslabor für Elektronenmikroskopie GFE), RWTH Aachen University is acknowledged for performing the EBSD analysis on PS-PVD samples.

References

[1] A. A. Evers, The hydrogen society. More than just a vision?, ISBN 978-3-937863-31-3, Hydrogeit Verlag, 16727 Oberkraemer, Germany 2010.

[2] W. Deibert, M. E. Ivanova, S. Baumann, O. Guillon, W.A. Meulenberg, Ion-conducting ceramic membrane reactors for high temperature applications, J. Membrane Sci. 543 (2017) 79-97.

[3] Arun C. Bose, Inorganic Membranes for Energy and Environmental Applications, Edt. A. C. Bose, ISBN: 978-0-387-34524-6, Springer Science+Business Media, LLC 2009.

[4] M. Marrony, H. Matsumoto, N. Fukatsu, M. Stoukides, Typical applications of proton ceramic cells: a way to market?, in Proton-conducting ceramics. From fundamentals to applied research, Edt. M. Marrony, by Pan Stanford Publishing Pte. Ltd., ISBN 978-981-4613-84-2 2016.

[5] P. Di Georgio, U. Desideri, Potential of reversible solid oxide cells as electricity storage system, Energies 9 (2016) 662-676.

[6] A. L. Dicks, D. A. J. Rand, Fuel cell systems explained, ISBN: 9781118613528, John Wiley & Sons Ltd.(2018)

[7] Y. Zheng, J. Wang, B. Yu, W. Yhang, J. Chen, J. Oiao, J. Yhang, A review of high temperature co-electrolysis of H_2O and CO_2 to produce sustainable fuels using solid

oxide electrolysis cells (SOECs): advanced materials and technology, Chem. Soc. Rev. 46 (2017) 1427-1463.

[8] M. Götz, J. Lefebre, F. Mörs, A. McDaniel Koch, F. Graf, S. Bajohr, R. Reimert, T. Kolb, Renewable power-to-gas: a technological and economic review, Renew. Energy 85 (2016) 1371-1390.

[9] Woodhead publishing series in energy, Nr. 76, Membrane reactors for energy applications and basic chemical production, Edt. A. Basile, L. Di Paola, F. I. Hai, V. Piemonte, by Elsevier Ltd, ISBN 978-1-78242-223-5 2015.

[10] S.H. Morejudo, R. Zanón, S. Escolástico, I. Yuste-Tirados, H. Malerod-Fjeld, P.K.Vestre, W.G. Coors, A. Martínez, T. Norby, J.M. Serra, C. Kjølseth, Direct conversion of methane to aromatics in a catalytic co-ionic membrane reactor, Science 353 (2016) 563-566.

[11] H. Malerod-Fjeld, D. Clark, I. Yuste-Tirados, R. Zanón, D. Catalán-Martínez, D. Beeaff, S.H. Morejudo, P.K. Vestre, T. Norby, R. Haugsrud, J.M. Serra, C. Kjølseth, Thermo-electrochemical production of compressed hydrogen from methane with near-zero energy loss, Nature Energy 2 (12) (2017) 923 - 931.

[12] E. Forster, dissertation, Thermal stability of ceramic membranes and catalysts for H_2-separation in CO-shift reactors, Energy and Environment Band, vol. 284, ISBN 978-3-95806-084-5, RUB 2015.

[13] S. Escolástico, V. Stournari, J. Malzbender, K. Haas-Santo, R. Dittmeyer, J.M. Serra, Chemical stability in H_2S and creep characterization of the mixed protonic conductor $Nd_{5.5}WO_{11.25-\delta}$, Int. J. Hydrogen Energy 43 (17) (2018) 8342-8354.

[14] C. Mortalò, E. Rebollo, S. Escolástico, S. Deambrosis, K. Haas-Santo, M. Rancan, R. Dittmeyer, L. Armelao, M. Fabrizio, Enhanced sulfur tolerance of $BaCe_{0.65}Zr_{0.20}Y_{0.15}O_{3-\delta}$-$Ce_{0.85}Gd_{0.15}O_{2-\delta}$ composite for hydrogen separation membranes, J. Membrane Sci. 564 (2018) 123-132.

[15] S. Escolástico, S. Somacescu, J. M. Serra, Tailoring mixed ionic-electronic conduction in H_2 permeable membranes based on the system $Nd_{5.5}W_{1-x}Mo_xO_{11.25-\delta}$, J. Mater. Chem. A 3 (2) (2015) 719-731.

[16] T. Shimura, S. Fujimoto, H. Iwahara, Proton conduction in non-perovskite-type oxides at elevated temperatures, Solid State Ionics 143 (2001) 117-123.

[17] D. van Holt, E. Forster, M. E. Ivanova, W. A. Meulenberg, M. Müller, S. Baumann, R. Vaßen, Ceramic materials for H_2 transport membranes applicable for gas separation under coal-gasification related conditions, J. Eur. Ceram. Soc. 34 (2014) 2381-2389.

[18] E. Forster, D. Van Holt, M. E. Ivanova, S. Baumann, W. A. Meulenberg, M. Müller, Stability of ceramic materials for H_2 transport membranes in gasification environment under the influence of gas contaminants, J. Eur. Ceram. Soc. 36 (2016) 3457-3464.

[19] S. Escolástico, C. Solís, T. Scherb, G. Schumacher, J. M. Serra, Hydrogen separation in $La_{5.5}WO_{11.25-\delta}$ membranes, J. Membrane Sci. 444 (2013) 276-284.

[20] S. Escolástico, J. Seeger, S. Roitsch, M. E. Ivanova, W. A. Meulenberg, J. M. Serra, Enhanced H_2 separation through mixed proton-electron conducting membranes based on $La_{5.5}W_{0.8}M_{0.2}O_{11.25-\delta}$, ChemSusChem 6 (2013) 1523-1532.

[21] A. Magrasó, C. Frontera, Comparison of the local and the average crystal structure of proton conducting lanthanum tungstate and the influence of molybdenum substitution, Dalton Trans. 45 (2016) 3791-3797.

[22] S. Escolástico, M. Schröder and J.M. Serra, Optimization of the Mixed Proton-Electronic Conducting Materials based on the $(Nd_{5/6}Ln_{1/6})_{5.5}WO_{11.25}$, J. Mater. Chem. A 2 (2014) 6616-6630

[23] R. Haugsrud, Defects and transport properties in Ln_6WO_{12} (Ln=La, Nd, Gd, Er), Solid State Ionics 178 (2007) 555-560.

[24] R. Haugsrud, C. Kjolseth, Effects of protons and acceptor substitution on the electrical conductivity of La_6WO_{12}, J. Phys. Chem. Solids 69 (2008) 1758-1765.

[25] A. Magrasó, C. Frontera, D. Marrero-López, P. Núñez, New crystal structure and characterization of lanthanum tungstate "La_6WO_{12}" prepared by freeze-drying synthesis, Dalton Trans. (2009) 10273-10283.

[26] A. Magrasó, J. Polfus, C. Frontera, J. Canales-Vázquez, L.-E. Kalland, C. Hervoches, S. Erdal, R. Hancke, M. Saiful Islam, T. Norby, R. Haugsrud, Complete structural model for lanthanum tungstate: a chemically stable high temperature proton conductor by means of instrinsic defects, J. Mater. Chem. 22 (2012) 1762-1764.

[27] T. Scherb, S. A.J. Kimber, C. Stephan, P. F. Henry, G. Schumacher, S. Escolástico, J.M. Serra, J. Seeger, J. Just, A. H. Hill, J. Banhart, Nanoscale order in the frustrated mixed conductor $La_{5.6}WO_{12-\delta}$, J. Appl. Cryst. 49 (2016) 997-1008.

[28] A. Fantin, T. Scherb, J. Seeger, G. Schumacher, U. Gerhards, M. E. Ivanova, W. A. Meulenberg, R. Dittmeyer, J. Banhart, Crystal structure of Re-substituted lanthanum tungstate $La_{5.4}W_{1-y}Re_yO_{12-\delta}$ ($0 \leq y \leq 0.2$) studied by neutron diffraction, J. Appl. Cryst. 49 (2016) 1544-1560.

[29] A. Fantin, T. Scherb, J. Seeger, G. Schumacher, U. Gerhards, M. E. Ivanova, W.A. Meulenberg, R. Dittmeyer, J. Banhart, Relation between composition and vacant oxygen

sites in the mixed ionic-electronic conductors $La_{5.4}W_{1-y}M_yO_{12-\delta}$ (M=Mo,Re; 0≤y≤0.2) and their mother compound $La_{6-x}WO_{12-\delta}$ (0.4≤x≤0.8), Solid State Ionics 306 (2017) 104-111.

[30] W.A. Meulenberg, M. E. Ivanova, H.P. Buchkremer, D. Stöver, J.M. Serra, S. Escolástico, CO_2 tolerant, mixed conductive oxide and uses thereof for hydrogen separation, US2013/0216938 A1 (2013)

[31] J. Seeger, M. E. Ivanova, W. A. Meulenberg, D. Sebold, D. Stöver, T. Scherb, G. Schumacher, S. Escolástico, C. Solís, J. M. Serra, Synthesis and characterization of nonsubstituted and substituted proton conducting $La_{6-x}WO_{12-\delta}$, Inorg. Chem. 52 (2013) 10375-10386.

[32] S. Escolástico, C. Solís, J.M. Serra, Study of H_2 permeation in $(La_{5/6}Nd_{1/6})_{5.5}WO_{12-\delta}$ membranes, Solid State Ionics 216 (2012) 31-35.

[33] M. Weirich, J. Gurauskis, V. Gil, K. Wiik, M.-A. Einarsrud, Preparation of lanthanum tungstate membranes by tape casting technique, Int. J. Hydrogen Energy, 37 (2012) 8056-8061.

[34] W. Deibert, M. E. Ivanova, W. A. Meulenberg, R. Vaßen, O. Guillon, Preparation and sintering behaviour of $La_{5.4}WO_{12-\delta}$ asymmetric membranes with optimized mictrostructure for H_2 separation, J. Membrane Sci. 492 (2015) 439-451.

[35] G. Mauer, R. Vaßen, D. Stöver, Thin and dense ceramic coatings by plasma spraying at very low pressure, J. Therm. Spray Technol. 19 (2010) 495-501.

[36] E. Bakan, R. Vaßen, Ceramic top coats of plsama-sprayed thermal barrier coatings: materials, processes, and properties, J. Therm. Spray Tech. 26 (2017) 992-1010.

[37] R. Dittmeyer, T. Boeltken, P. Piermartini, M. Selinsek, M. Loewert, F. Dallmann, H. Kreuder, M. Cholewa, A. Wunsch, M. Belimov, S. Farsi, P. Pfeifer, Micro and micro membrane reactors for advanced application in chemical energy conversion, Curr. Opin. Chem. Eng. 17 (2017) 108-125

[38] S. Escolástico, V.B. Vert, J.M. Serra, Preparation and characterizationof nanocrystalline mixed proton-electronic conducting materials based on the system La_6WO_{12}, Chem. Mater. 21 (2009) 3079-3089.

[39] V. Gil, R. A. Strøm, L. J. Groven and M.-A. Einarsrud, $La_{28-x}W_{4+x}O_{54+3x/2}$ powder prepared by spray pyrolysis, J. Am. Ceram. Soc. 95 (2012) 3403-3407.

[40] W. Deibert, F. Schulze-Küppers, E. Forster, M. E. Ivanova, M. Müller, W. A. Meulenberg, Stability and sintering of MgO as a substrate materials for Lanthanum tungstate membranes, J. Eur. Ceram. Soc. 37 (2017) 671-677.

[41] M.O. Jarligo, G. Mauer, M. Bram, S. Baumann, R. Vaßen, Plasma Spray Physical Vapor

Deposition of $La_{1-x}Sr_xCo_yFe_{1-y}O_{3-\delta}$ thin-film oxygen transport membrane on porous metallic supports, J. Therm. Spray Technol. 23 (2014) 213-219.

[42] D. Marcano, G. Mauer, Y.J. Sohn, R. Vaßen, J. Garcia-Fayos, J.M. Serra, Controlling the stress state of $La_{1-x}Sr_xCo_yFe_{1-y}O_{3-\delta}$ oxygen transport membranes on porous metallic supports deposited by plasma spray-physical vapor process, J. Membrane Sci. 503 (2016) 1-7.

[43] D. Marcano, G. Mauer, R. Vaßen, A. Weber, Manufacturing of high performance solid oxide fuel cells (SOFCs) with atmospheric plasma spraying (APS) and plasma spray-physical vapor deposition (PS-PVD), Surf. Coatings Technol. 318 (2017) 170–177.

[44] S. Brunauer, P. Emmett, E. Teller, Adsorption of Gases in Multimolecular Layers, J. Am. Chem. Soc. 60 (1938) 309-319.

[45] M. Amsif, A. Magrasó, D. Marrero-Lopey, J. C. Ruiz-Morales, J. Canales-Vazquez, P. Nunez, Mo-substituted Lanthanum tungstate: a competitive mixed electron-proton conductor for gas separation membrane applications, Chem. Mater. 24 (2012) 3868-3877.

[46] D. Marcano, G. Mauer, Y. J. Sohn, A. Schwedt, M.Bram, M. E. Ivanova, R. Vaßen, Plasma Spray-Physical Vapor Deposition of single phase Lanthanum tungstate for hydrogen gas separation membranes, t.b. submitted (2018).

[47] M. E. Ivanova, S. Escolático, M. Balaguer, J. Palisaitis, Y. J. Sohn, W.A. Meulenberg, O. Guillon, J. Mayer, J.M. Serra, Hydrogen separation through tailored dual phase membranes with nominal composition $BaCe_{0.8}Eu_{0.2}O_{3-\delta}$:$Ce_{0.8}Y_{0.2}O_{2-\delta}$ at intermediate temperatures, Sci. Rep. 6 (2016) 34773-34787.

[48] S. Escolástico, M. E. Ivanova, C. Solís, S. Roitsch, W.A. Meulenberg, J.M. Serra, Improvement of transport properties and hydrogen permeation of chemically-stable proton-conducting oxides based on the system $BaZr_{1-x-y}Y_xM_yO_{3-\delta}$, RSC Adv. 2 (2012) 4932-4943.

[49] E. Rebollo, C. Mortalò, S. Escolástico, S. Boldrini, S. Barison, J.M. Serra, M. Fabrizio, Exceptional hydrogen permeation of all-ceramic composite robust membranes based on $BaCe_{0.65}Zr_{0.2}Y_{0.15}O_{3-\delta}$ and Y- or Gd-doped ceria, Energy Environ. Sci. 8 (2015) 3675-3686.

[50] D. Montaleone, E. Mercadelli, S. Escolástico, A. Gondolini, J.M. Serra, A. Sanson, All-ceramic asymmetric membranes with superior hydrogen permeation, J. Mater. Chem. A, (2018), http://dx.doi.org/10.1039/C8TA04764B.